

Ultralong Period Seismic Study of the December 2004 Indian Ocean Earthquake and Implications for Regional Tectonics and the Subduction Process

by Seth Stein and Emile A. Okal

Abstract Analysis of the earth's longest period normal modes shows that the December 2004 Sumatra–Andaman earthquake was much larger (M_w 9.3) than initially inferred from surface-wave data and involved slip on a much longer fault than initially inferred from body-wave data. The seismic moment and relative excitation of the normal modes indicate that the entire aftershock zone ruptured, consistent with the large tsunami amplitudes in Thailand, Sri Lanka, and India. An apparent increase in seismic moment with period results from interference between parts of the fault. The earthquake resulted from subduction of the Indian plate beneath the Burma microplate, a sliver plate between the Indian and Sunda plates. Hence, the rate and direction of convergence depends on the motion of the Burma plate, which is not well known. Convergence would be highly oblique if the rate of motion between Burma and Sunda is that inferred from spreading in the Andaman Sea, and less if a slower rate is inferred from the Sagaing fault. The December earthquake was much larger than expected from a previously proposed relation, based on the idea of seismic coupling, in which such earthquakes occur only when young lithosphere subducts rapidly. Moreover, a global reanalysis finds little support for this correlation. Hence, we suspect that much of the apparent differences between subduction zones, such as some trench segments but not others being prone to $M_w > 8.5$ events and hence oceanwide tsunamis, may reflect the short earthquake history sampled. This possibility is supported by the variability in rupture mode at individual trench segments.

Introduction

The 26 December 2004 Sumatra–Andaman (or “Sumatra”) earthquake was the first “giant” or “extreme” (moment magnitude $M_w \geq 9$) earthquake since the 1964 Alaskan event. Its enormous size and the devastating tsunami that resulted prompted a wide range of studies by earth scientists world wide. These studies were greatly facilitated by the availability in near-real time of high-quality seismological, geodetic, and other geophysical data. Information became rapidly available, making this the best-studied earthquake of its size and providing a basis for studies that will likely continue for many years.

Our purpose here is to extend our initial study of the earthquake by using the earth's longest-period normal modes. This study (Stein and Okal, 2005), published three months after the event, showed that the earthquake was much larger and involved slip on a much longer fault than at first thought. This analysis provided insight into the generation of the tsunami, the recurrence time of similar earthquakes, and the regional tectonics. Our subsequent studies and those of many other investigators (e.g., Banerjee *et al.*,

2005; Ni *et al.*, 2005; Park *et al.*, 2005; Tsai *et al.*, 2005; Vigny *et al.*, 2005) in general support these initial findings and provide considerably more information. Hence, we extend our initial results in the light of subsequent studies both of the December earthquake and the M_w 8.7 Simeulue–Nias earthquake that occurred on 28 March 2005 on a segment of the trench immediately to the south.

The Sumatra earthquake also provides an impetus to re-examine ideas about the conditions required for such giant events. It has long been recognized that subduction zones differ in many ways, including the fact that (at least on the short timescales over which we have observations), some have much larger and more common earthquakes at the thrust fault interface between the overriding and subducting plates. As a result, considerable effort has gone into trying to characterize this variation and interpret it in terms of the physical properties and stress state of the interface. A particularly important question is whether such earthquakes can occur at any subduction zone, or whether certain combinations of convergence rate, age of the subducting plate, or

trench sediment thickness (Ruff and Kanamori, 1980; Ruff, 1989) are required.

This issue is important for assessing tsunami hazards and improving tsunami-warning systems. As summarized in Figure 1, the danger of an oceanwide or far-field (as opposed to local) tsunami is low for earthquakes with $M_w < 8.5$, significant for earthquakes with larger moment magnitude, and becomes extreme for $M_w \geq 9$. Hence neither body-wave magnitude m_b , nor surface-wave magnitude M_s , the most traditional measures of earthquake size easily determined in the first few minutes after a major earthquake, are suitable for tsunami warning.

This limitation arises from the spectra of earthquake sources. In theory, a plot of the logarithm of amplitude of the radiated waves versus the logarithm of the frequency is flat at low frequency (long period) with amplitude proportional to the static moment M_0 , and then decays for periods shorter than the rupture time T_R needed for the rupture to propagate along the length of the fault and the rise time T_D needed for slip to be completed at a point on the rupture. Thus, once earthquakes reach a certain size, both m_b , measured around a period of 1 sec, and M_s , measured at 20 sec, saturate and do not exceed about 6.3 and 8.2, respectively (Geller, 1976). This effect prompted development of the moment magnitude which is calculated from the seismic moment (in dyne cm) using $M_w = (\log M_0/1.5) - 10.73$ (Hanks and Kanamori, 1979), and defined so that the moment magnitude correlates with the other magnitudes when they have not fully saturated.

Magnitude saturation is a serious problem for tsunami warning because “great” earthquakes, traditionally defined as ones with $M_s \geq 8$, can be either too small to generate an ocean wide tsunami, or large enough that the risk is great. As a result, algorithms have been developed to more rapidly

assess the seismic moment (Okal and Talandier, 1989; Tsuboi *et al.*, 1995; Weinstein and Okal, 2005) and decide if a warning should be issued. The first crucial hours after the Sumatra earthquake illustrate the challenge (Kerr, 2005a). The Pacific Tsunami Warning Center’s first bulletin, 15 min after the earthquake, estimated its magnitude using long-period body waves (not m_b) at M_{wp} 8.0, with little risk of an oceanwide tsunami. Forty-five minutes later, using mantle-wave data, the estimate was raised to 8.5, for which an oceanwide tsunami was likely. Four hours after the event, the Harvard Centroid Moment Tensor (CMT) project used longer-period surface waves to infer a moment magnitude of 9.0, for which the tsunami risk would have been recognized to be very high. By then, the coasts of Thailand and Sri Lanka lay devastated.

Figure 2 summarizes the information about the earthquake source available within a few days after the earthquake. The first day’s aftershock zone extended 1200 km northward along the Sumatra trench from the epicenter off Sumatra (3.3° N, 95.8° E) to the Andaman Islands. The Harvard CMT solution showed a nearly pure thrust mechanism, and using surface waves with period up to 300 sec found M_0 4×10^{29} dyne cm, corresponding to M_w 9.0. Initial body wave inversions (*e.g.*, Ji, 2005) found that rupture started at the epicenter at the south end of this zone and propagated northward, but was limited to the southern third of the aftershock zone.

The result that most slip occurred on the southern portion of the aftershock zone was surprising for two reasons. First, aftershocks occurring within the first day after great subduction-zone earthquakes in general are assumed to delineate the rupture area (Kanamori, 1977a). Second, because tsunami amplitudes are largest perpendicular to the fault, slip limited to the southern northwest-trending portion of the af-

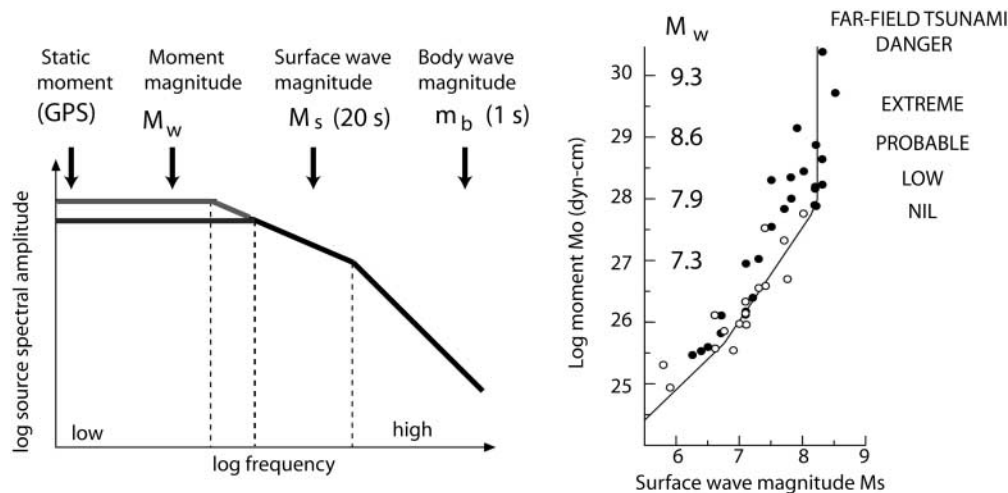


Figure 1. (Left) Schematic source spectrum illustrating frequencies at which various magnitudes are measured. Both m_b and M_s saturate for great earthquakes. (Right) As a result, M_s does not adequately represent the size or tsunamigenic potential of great earthquakes (after Geller, 1976).

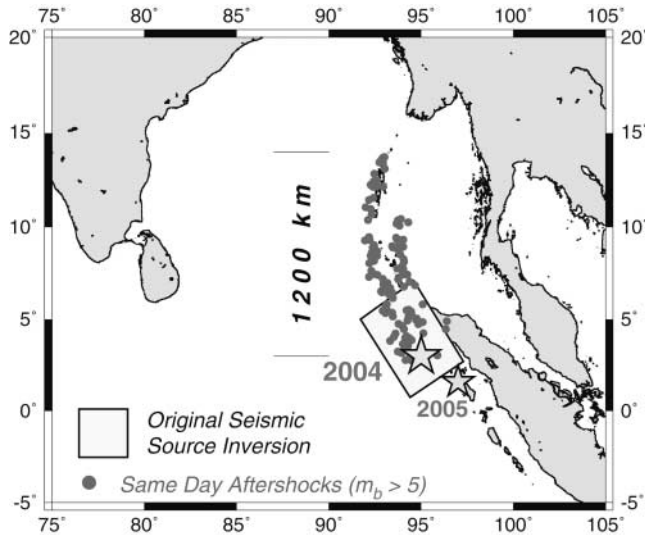


Figure 2. Regional setting of the 2004 Sumatra–Andaman and 2005 Simeulue–Nias earthquakes. Epicenters shown by stars. Shaded rectangle shows source extent from initial body-wave inversion (Ji, 2005). Dots represent the same-day aftershocks of the 2004 event, defining a much larger fault zone, extending 1200 km north along the trench.

tershock zone would not have been expected to produce the large tsunami amplitudes in Thailand, Sri Lanka, and India.

Initial Results

Our analysis took an alternative approach by using the earth’s longest-period normal modes. Fourier analysis of long seismic records showed split modes, illustrated in Figure 3 for the five singlets making up the ${}_0S_2$ multiplet, the earth’s fundamental mode with period 3232 sec. The records also showed beautifully split ${}_0S_3$ and ${}_0S_4$ multiplets. We modeled these multiplets, using Stein and Geller’s (1977) approach, which includes the effects of rotation and ellipticity, but not lateral heterogeneity. We also modeled radial modes ${}_0S_0$ and ${}_1S_0$ which contain only one singlet and thus are not split. We used the focal mechanism and depth reported by the Harvard CMT project and singlet eigenfrequencies including the effects of rotation and ellipticity. We obtained consistent estimates of seismic moment and Q for ${}_0S_2$, ${}_0S_3$, and ${}_0S_4$ in both the time and frequency domains. The moment measured for ${}_0S_2$, 1×10^{30} dyne cm, is approximately three times larger than measured from 300-sec surface waves, giving a magnitude M_w of 9.3, significantly larger than the previously reported M_w 9.0.

Our interpretation of these results was that faulting had occurred along the entire aftershock zone, rather than only its southern third (Stein and Okal, 2005). This larger moment was consistent with 11 m of slip on a fault 1200 km long and 200 km wide (down-dip dimension). A longer rupture is also consistent with the fact that split modes are better fit by a source with centroid at 7° N than by one at the epicenter

at 3° N, where rupture started and propagated northward (Fig. 4).

This interpretation was also consistent with several key tsunami observations. The large tsunami amplitudes in Sri Lanka and India also favor rupture on the northern, north-trending, segment because tsunami amplitudes are largest perpendicular to the fault. This effect is due to directivity, the amplitude variation with azimuth due to radiation from a moving source. The amplitude varies with azimuth ϕ from the fault strike as

$$\text{sinc}(X) = \frac{\sin X}{X} \quad \text{where } X = \frac{\omega L}{2c} (c/V_R - \cos \phi)$$

where L is fault length, c is the radiated phase velocity, and V_R is the velocity of rupture (Aki and Richards, 1980). For seismic waves, c/V_R is about 1, so the maximum amplitude is along the direction of rupture propagation. In contrast, the tsunami speed under the shallow-water approximation, $(gh)^{1/2}$ is about 200 m/sec for a depth $h = 4$ km, much slower than the rupture velocity of about 2.8 km/sec. As a result, $c/V_R \ll 1$, and the amplitude is largest at right angles to the fault (Ben-Menahem and Rosenman, 1972). Hence modeling the tsunami assuming that slip occurred along the entire fault predicts larger amplitudes in Sri Lanka and India than assuming only slip on its southern part (Fig. 5).

Subsequent Results

We and a subsequent analysis by Park *et al.* (2005) were left with a puzzling initial result, a systematic increase of moment with increasing period (Fig. 6). We interpreted this as a consequence of the fact that the normal-mode solution found a larger moment and longer fault than the initial body- and surface-wave studies, implying that slow rupture had taken place on the northern two-thirds of the aftershock zone.

Hence, we began this study by attempting to model this effect as a direct consequence of the fault size. As shown in Figure 6 (top), the moment increased with period approximately as $T^{-0.4}$, or decayed with frequency as $\omega^{-0.4}$. However, source theory predicts ω^{-1} decay from the static moment (Fig. 1) for frequencies above the first corner frequency. Although simple models assuming various source durations predict a general increase in moment with period, they do not fit the moment values well, as illustrated in Figure 7 using simple “boxcar” models of constant moment rate release regularly spread over a duration D :

$$\dot{M}_0(t) = \frac{M_0}{D} \quad (0 \leq t < D); \quad \dot{M}_0(t) = 0 \quad \text{otherwise.}$$

This model makes no direct assumption of any rupture slowness. The amplitude of its Fourier transform at angular frequency ω is $\text{sinc}(\omega D/2)$, which is plotted in logarithmic

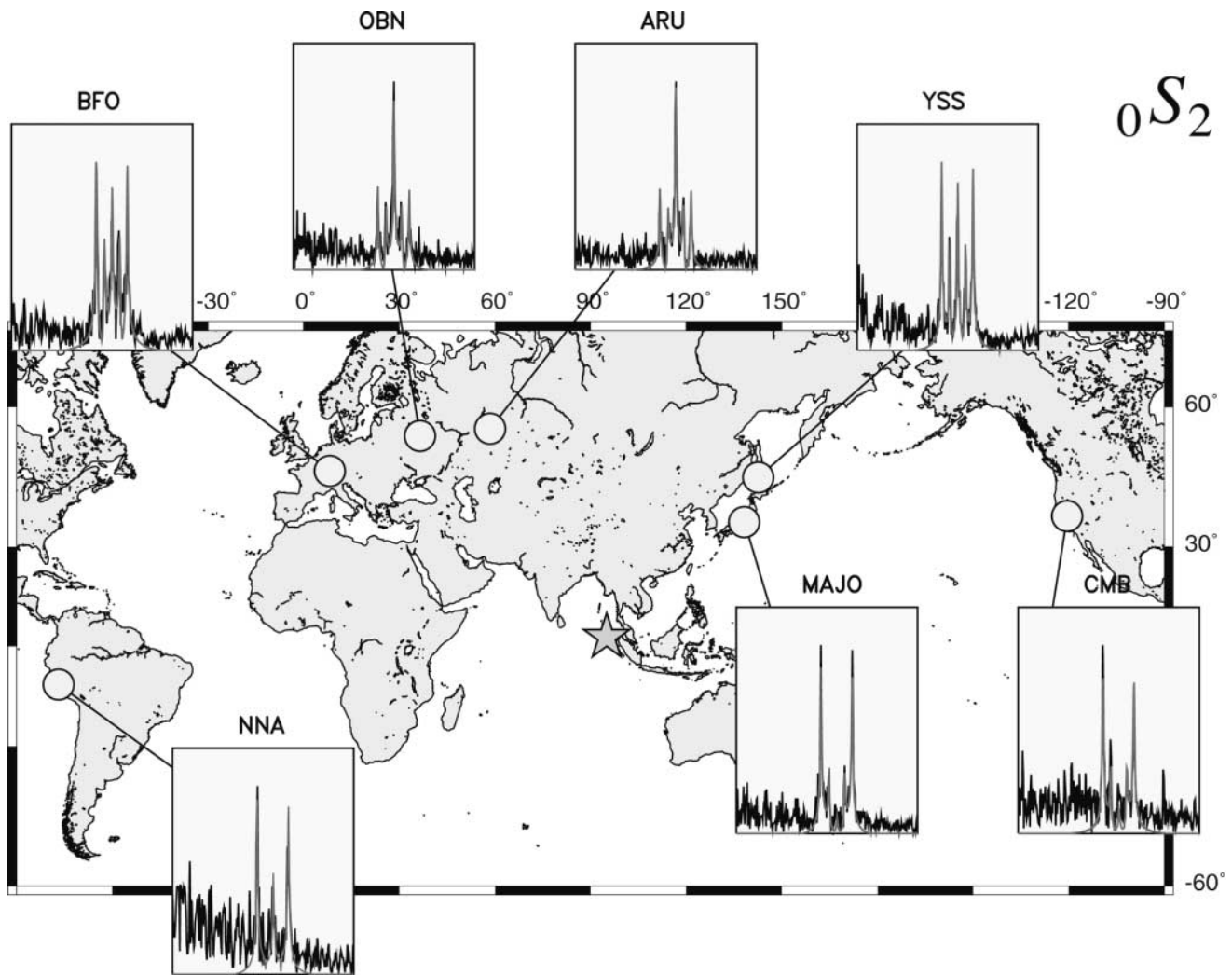


Figure 3. Amplitude spectra of ${}_0S_2$ at seven stations. Note the control of the splitting pattern by receiver latitude. Stations with comparable latitudes (BFO and YSS, OBN and ARU, MAJO and CMB) show similar excitation of singlets.

coordinates for source durations ranging from 200 to 800 sec. None of these models explains the full set of best-fitting moments. A short duration of 200 sec would reconcile the 300-sec CMT solution with the gravest modes, but would misfit ${}_0S_0$ and especially ${}_1S_0$, whereas longer durations would misfit the CMT solution. A satisfactory model must therefore involve a more complex behavior of the source, in which the moment rate release varies more irregularly with time.

The increase in moment with increasing period also did not appear to be a result of the fault dip assumed. Although the absolute moment inferred trades off with dip (Fig. 8), both for the normal-mode and CMT solutions, the relative moments between the different modes would be unaffected.

These issues have become clearer due to many results reported simultaneously with, and subsequent to, our first article's publication (31 March 2005). Analyses using body waves (Ammon *et al.*, 2005; Ishii *et al.*, 2005; Ni *et al.*, 2005), surface waves (Lay *et al.*, 2005; Tsai *et al.*, 2005),

normal modes (Park *et al.*, 2005), GPS (Banerjee *et al.*, 2005; Vigny *et al.*, 2005), and hydrophones (deGroot-Hedlin, 2005; Guilbert *et al.*, 2005; Tolstoy and Bohnenstiehl, 2005) all found that rupture extended along the entire aftershock zone.

We thus modeled the data by generating synthetic normal mode seismograms for a set of point sources using Tsai *et al.*'s (2005) composite CMT source model of five sources offset in time along the rupture with varying amplitudes and focal mechanisms. This solution gives an excellent fit to the normal mode data (Fig. 9) with a total moment of 1.2×10^{30} dyne cm, corresponding to M_w 9.3 and consistent with Tsai *et al.*'s (2005) surface-wave value. Hence the total moment remains approximately three times that inferred from the initial CMT solution. However, the increase in moment with period we had inferred using a single point source model is no longer required, because it results from interference between energy radiated from parts of the fault,

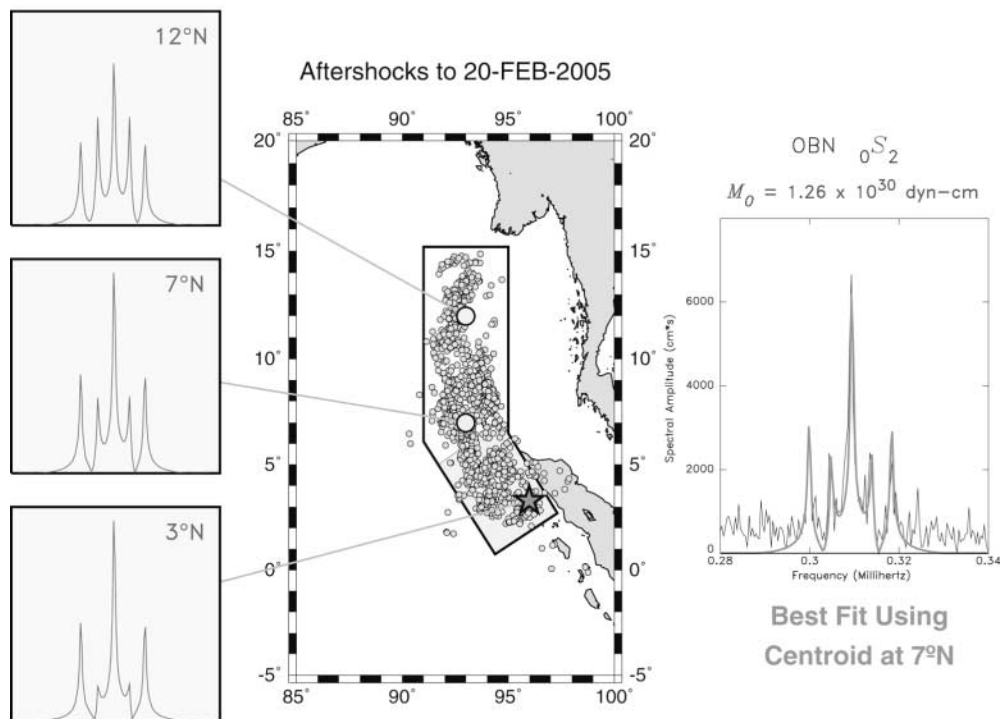


Figure 4. Split-singlet pattern for ${}_0S_2$ showing dependence on source latitude. Map at the center illustrates the two possible models of source rupture: the short fault initially inferred from body-wave inversion (shaded block) and the long fault (open block) suggested by the distributions of aftershocks (small circles). The diagrams at left show theoretical splitting patterns at Obninsk, Russia (OBN), for sources located at the original U.S. Geological Survey epicenter (3° N; star), at 7° N, and toward the northern end of the long fault (12° N). The right-hand panel shows the best fit between data (thin black line) and synthetic (thick gray line), obtained for a centroid of moment release at 7° N, at the center of the aftershock zone but outside the rupture zone of the short-fault model.

rather than purely from the fault size. Tsai *et al.*'s (2005) model implies an irregular rupture velocity, varying from 4 km/sec to less than 2 km/sec. The average velocity, 2.8 km/sec, is somewhat slower than typical values (about 2.5–3.5 km/sec) without, however, reaching the very low values (1 km/sec) observed for so-called tsunami earthquakes (Polet and Kanamori, 2000; López and Okal, 2006). This irregularity in rupture velocity and in geographic distribution of moment release is why simple duration models fail to account for the apparent increase of moment with period. It also explains why a similar increase did not occur for the 28 March earthquake, which was smaller but in a similar location and with a similar fault geometry (Fig. 6, bottom).

In our view, the crucial result is not the precise value of the moment or moment magnitude. The Sumatra earthquake, which is the most studied large earthquake to date with the best and most diverse data, demonstrates again that these quantities have uncertainties (typically 0.1–0.2 units in moment magnitude) owing to the data type, specific data used, and assumptions required in the analysis. As in most such situations, the true uncertainty will reflect the systematic errors that exceed the formal uncertainty associated with

measurements from a specific set of data with a specific technique. Hence whether the earthquake's "real" magnitude is 9.2 or 9.3 is not the issue. The important point, as discussed next, is that the entire aftershock zone ruptured.

Plate Motions and Earthquake Recurrence

The view emerging from the normal modes and other seismological studies gives interesting insight into the regional tectonics and the recurrence interval of such giant earthquakes.

Unlike its 1960 Chile and 1964 Alaska cousins, the Sumatra earthquake occurred in a complex and poorly understood tectonic setting (Fig. 10). In a mega-sense, the earthquake is related to the collision between the Indian and Eurasian plates. As a result, it is natural to think of the earthquake as releasing strain accumulated at the Sumatra trench by the ~ 40 mm/yr of northeastward motion of India with respect to Eurasia. However, the actual plate geometry and motions are complex and not well known. One complication is that much of southeast Asia, including Thailand, the Malay Peninsula, and the South China Sea is presently viewed

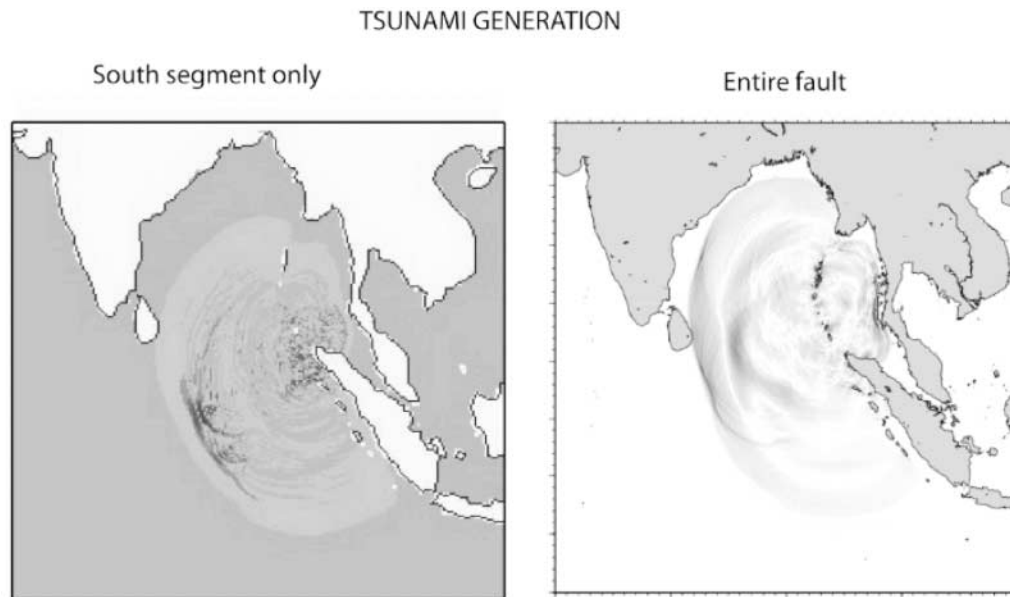


Figure 5. Comparison of predicted tsunami amplitudes 100 min after the origin time assuming the entire fault ruptured (<http://staff.aist.go.jp/kenji.satake/animation.gif>) or only the southern segment did (www.nio.org/jsp/tsu_simu.htm). Tsunami amplitudes would have been lower in Thailand, Sri Lanka, and India if only the southern segment of the fault had ruptured.

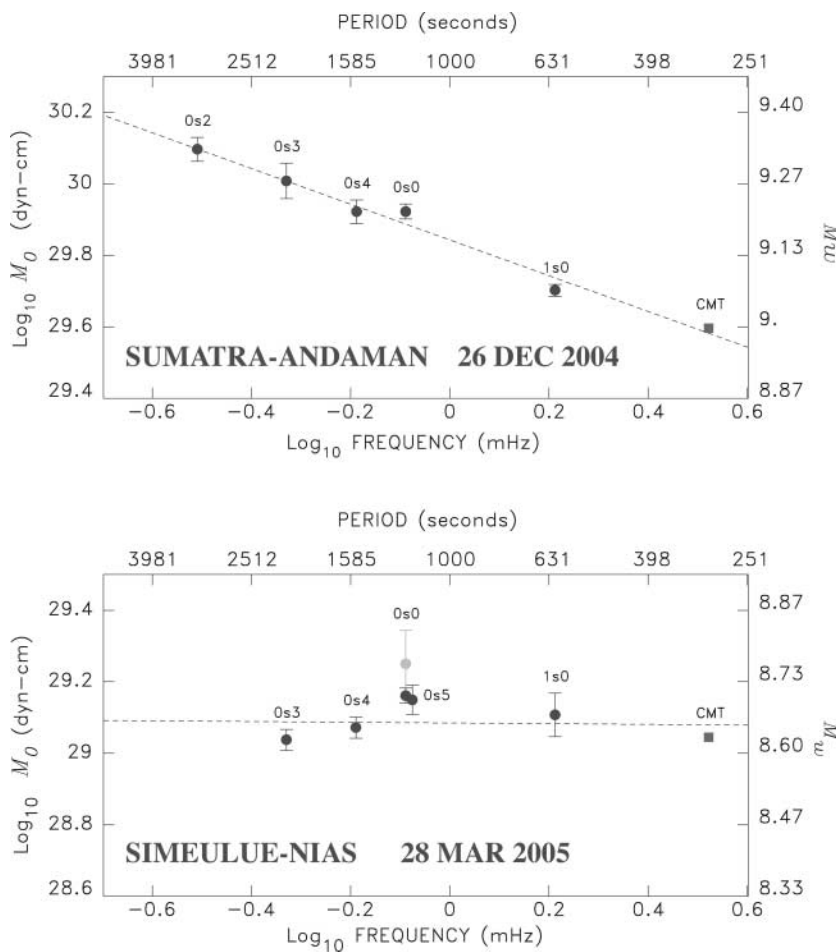


Figure 6. (Top) Best-fitting moments as a function of multiplet frequency for the 2004 Sumatra–Andaman earthquake. Individual dots (with error bars) are values derived from Figures 4 and 5 using a single point source double-couple source. Square shows CMT solution obtained at 300 sec. The moment systematically increases with increasing period. (Bottom) Same as top for 2005 Simeulue–Nias event. In this case, ${}_0S_2$ does not emerge from noise level and ${}_0S_0$ must be fit with a 83-day time series because a shorter one (gray symbols) overestimates the moment. The moment from the single source CMT solution fits all the modes.

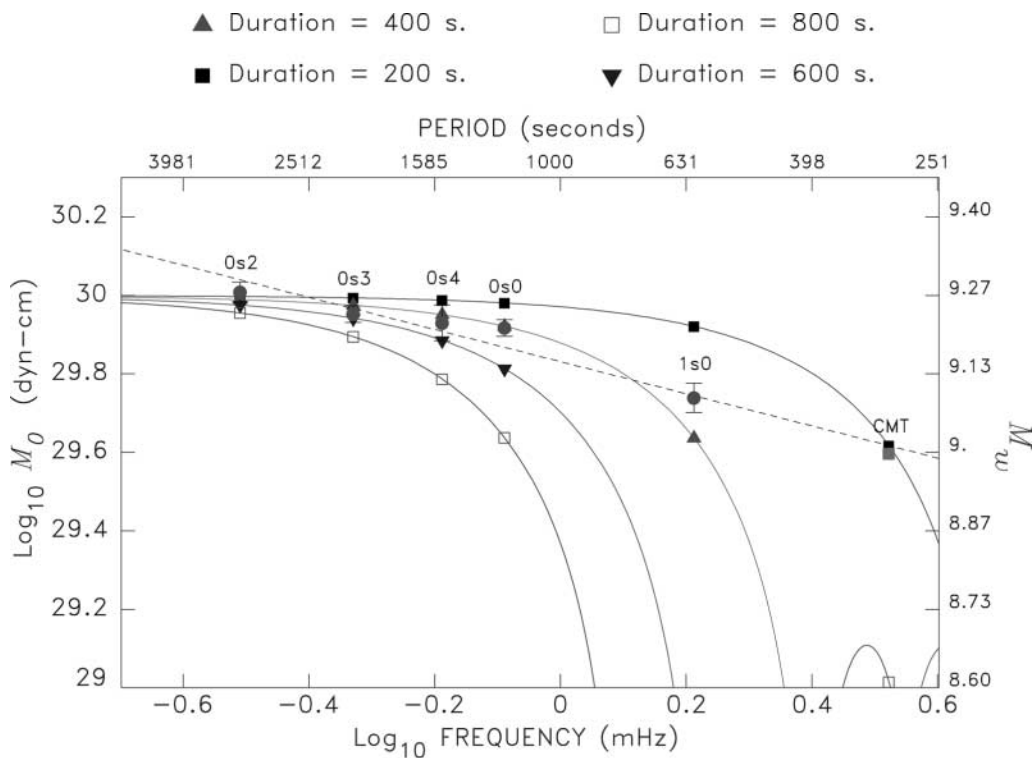


Figure 7. Attempt to fit the observed variations in resolved moment with a simple boxcar function of variable duration D . Curves for several values of D (squares and triangles at the modal frequencies) are superimposed on data of Figure 6 (top). As detailed in the text, none of the curves reconcile the entire dataset.

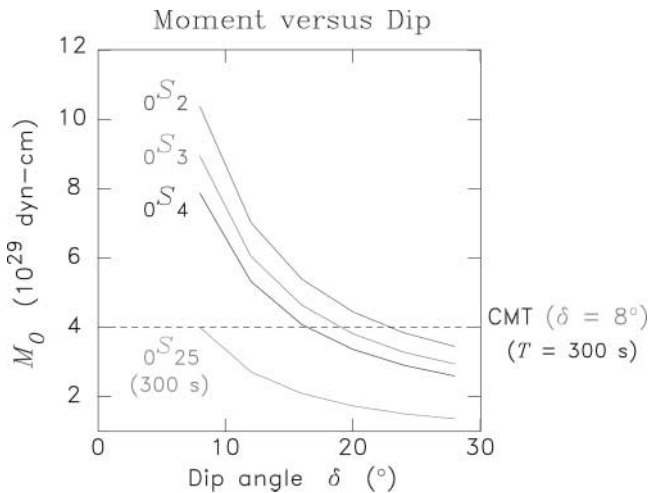


Figure 8. Trade-off between absolute moment and dip illustrated by the best-fitting moment for the three gravest spheroidal modes, as a function of the dip angle of a point source double-couple. Although the absolute values of the moment depend on δ , for all values of dip, the relative moments remain incompatible between themselves and even more so with the excitation of the 300-sec waves used in the initial Harvard CMT inversion (lower trace, equivalent to $0S_{25}$).

as forming the Sunda plate. Global Positioning System (GPS) data show that Sunda moves relative to Eurasia and is thus a distinct plate (Chamot-Rooke and Le Pichon, 1999; Michel *et al.*, 2001). A second complication is that the oceanic lithosphere subducting at the trench consists of the Indian plate to the north, the Australian plate to the south, and possibly a diffuse boundary between them extending as far north as about 10° N (Royer and Gordon, 1997). Hence, some of the subducting plate involved in the December 2004 event might be regarded as part of Australia, but for simplicity we do not do so.

The most crucial complication is that between the subducting Indian plate and the Sunda plate is the Burma microplate, a sliver plate. The presence of a distinct Burma microplate is shown by magnetic anomalies at the Andaman spreading center recording active seafloor spreading at 37 mm/yr between the Burma and Sunda plates (Curry *et al.*, 1979; Raju *et al.*, 2004). This relative motion is also shown by normal-faulting earthquakes on the Andaman spreading center (Guzman-Speziale and Ni, 1993) and strike-slip events on the major transform zone to the south that connects the Andaman spreading center to the Sumatra fault. It is intriguing that after the December earthquake both strike-slip and normal-fault earthquakes occurred on this feature (M. Nettles, personal comm.) A component of extension across it, or short spreading segments within it (Curry *et al.*,

COMPOSITE SOLUTION

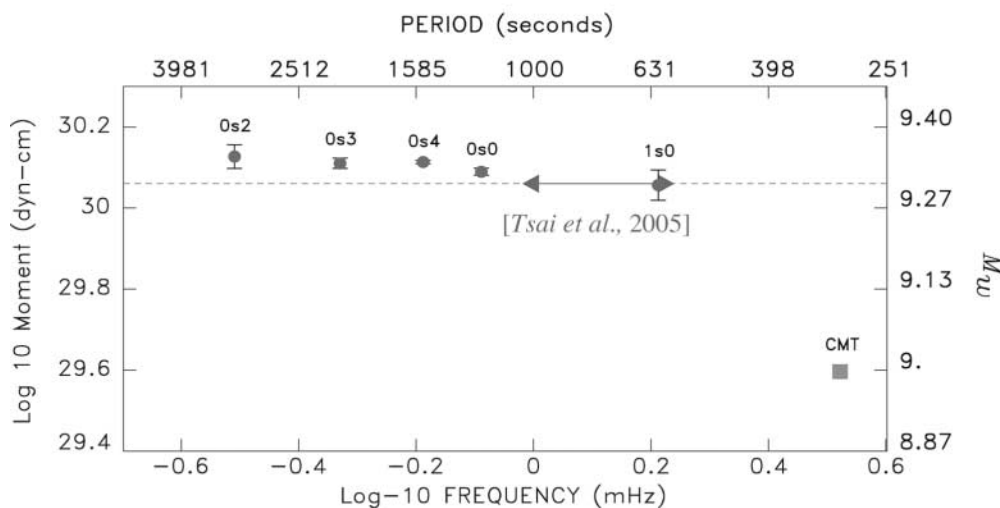
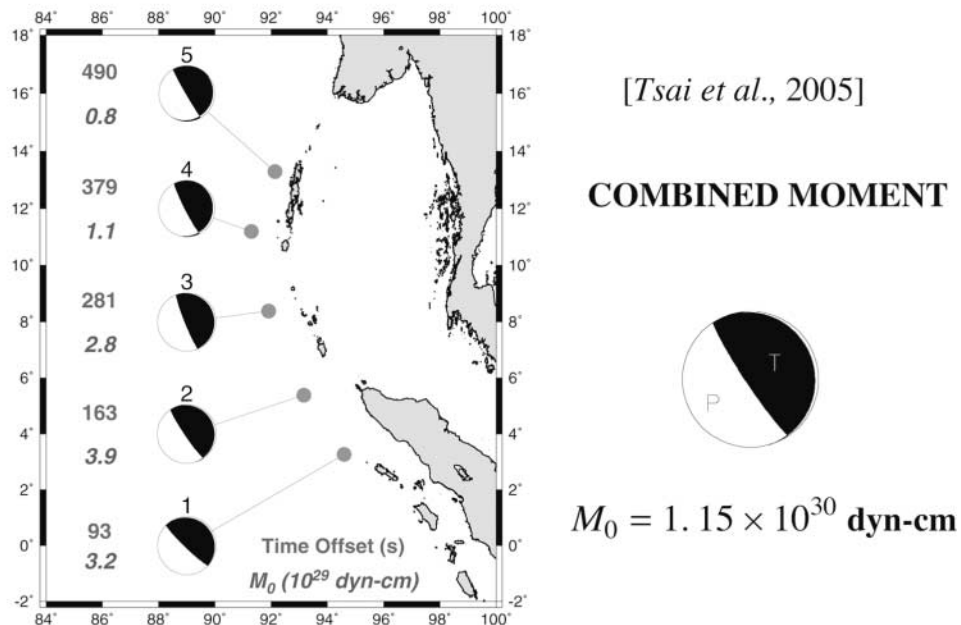


Figure 9. (Top) Composite CMT solution of the 2004 Sumatra earthquake, inverted between 600 and 1000 sec by Tsai et al. (2005). The map shows the spatiotemporal offset of the five sources, and the best-fitting double-couple resulting from their sum at zero frequency is shown at the right. (Bottom) Modeling of the dataset using the composite source. For each mode, only the total seismic moment is allowed to vary, while all other parameters of the five sources are fixed. The resulting best-fitting moments (solid dots) are consistent between modes and agree with Tsai et al.'s (2005) value. Note the excellent agreement of all modes with these authors' final solution.

1979), would be consistent with the mechanisms and its trend's deviation from the assumed spreading direction orthogonal to the spreading axis and parallel to the short transforms bounding the axis.

However, the extent of the Burma plate is unclear. Cur-ray et al. (1979) include both the oceanic region between

the Andaman spreading center and the Sumatra trench, and the region on land between the Burma arc and Sagaing fault. In this geometry, the Burma arc is an India-Burma subduction zone (Ni et al., 1989; Holt et al., 1991; Satyabala, 2003) and the Sagaing fault is a Burma-Sunda transform (Nielson et al., 2004). Bird (2003), however, considers the land area

north of about 15° N on both sides of the Sagaing fault to be a broad deforming region, not part of either the Burma or Sunda plates. Bird's (2003) geometry is easier to visualize because the 18 mm/yr of strike-slip motion on the Sagaing fault measured using GPS (Vigny *et al.*, 2003) and its trend are not compatible with the rate and direction of Burma–Sunda motion inferred from the magnetic data and transform trends. Because in this geometry the “Burma” plate does not include Burma, it might better be called the “Andaman” plate except for the risk of creating even more confusion. There is also discussion about where (presumably on Sumatra) the south end of the Burma plate is.

Even with these complexities, it seems that most or all

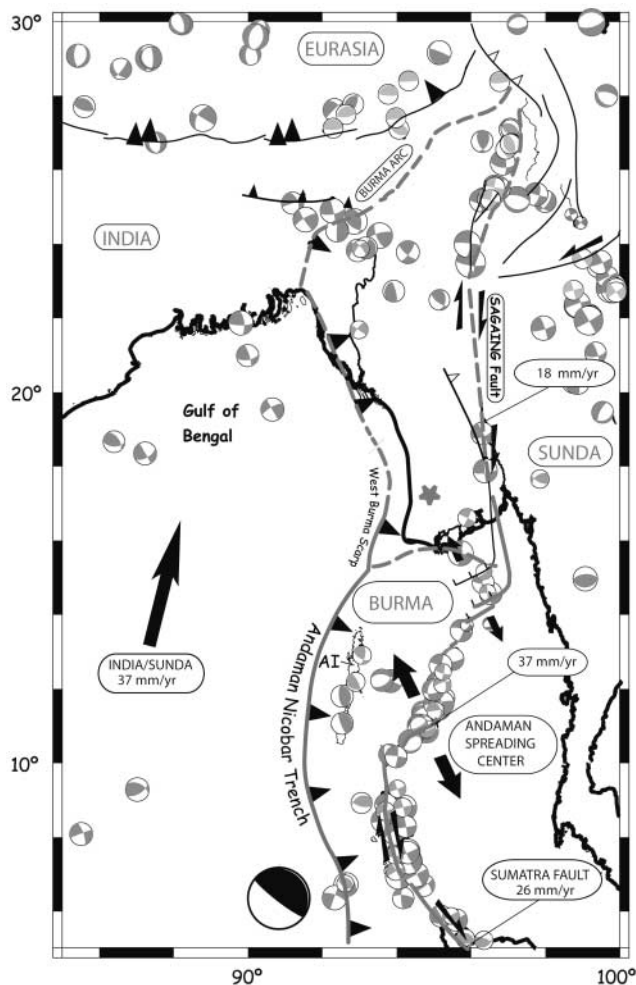


Figure 10. Regional setting of the Burma microplate and surroundings. Solid line shows Burma plate geometry in Bird (2003) model; dashed line shows northern extension in Curray *et al.* (1979) model. Note that the rate and direction of Burma–Sunda motion inferred from magnetic anomalies and transform trends on the Andaman spreading center are incompatible with the trend of, and rate across, the Sagaing fault. Star shows India–Burma pole inferred from Bird's (2003) Burma–Sunda Euler vector. Modified from Nielson *et al.* (2004).

of the convergence at the portion of the Sumatra trench that broke in the December 2004 earthquake is between the subducting Indian and overriding Burma plates. To estimate the motion between the Indian and Burma plates, we use a procedure similar to that in our initial study (Stein and Okal, 2005). We first find the motions of the major plates from the differences between Euler vectors determined from GPS data in the International Terrestrial Reference Frame (ITRF) for the motions of Sunda (Vigny *et al.*, 2003), India, Australia, and Eurasia (Sella *et al.*, 2002). In doing so, we neglect small differences resulting from the former being in ITRF-2000 and the latter in ITRF-97.

Although all of these Euler vectors have uncertainties, the biggest challenge is constraining Burma's motion with respect to Sunda. The rate of back-arc spreading is known only across one ridge segment. The only directional data are transform segments, which do not give consistent trends. The short transforms bounding the spreading segment imply relative motion oriented about 153°, as would assuming motion in the direction orthogonal to the ridge. Because this azimuth is insufficient to constrain the location of the Euler pole, Curray *et al.* (1979) and Bird (2003) used additional directional assumptions based on the regional plate geometry to estimate Euler vectors. Although these Euler vectors differ, both are constrained by the spreading rate and transform azimuth and so make similar predictions along the nearby trench.

We used Euler vectors of both Curray *et al.* (1979) and Bird (2003) to infer India's motion with respect to Burma (Table 1). The pole derived from Bird's Burma–Sunda motion is somewhat north of both our earlier estimate, which averaged the Bird and Curray *et al.* Euler vectors, and Bird's

Table 1
Euler Vectors

Plate Pair	Pole		ω (deg/m.y.)	Ref.
	Lat. (° N)	Lon. (° E)		
SU-BB	13.9	103.7	2.1	*
SU-BC	23.86	125.12	0.64	†
IN-IT	53.65	-13.99	0.483	‡
EU-IT	58.27	-102.21	0.257	‡
SU-IT	-59.0	81.0	-0.303	§
SU-EU	61.40	-79.27	0.047	
IN-EU	28.58	11.60	0.356	
BB-EU	-12.67	-76.33	2.112	
BC-EU	-19.77	-55.75	0.644	
IN-BB	17.00	95.00	2.168	
IN-BC	34.50	93.50	0.685	
IN-SU	22.38	15.70	0.339	

First plate moves counterclockwise with respect to the second.

Plate names: SU, Sunda; IN, India; EU, Eurasia.

*Bird (2003). BB denotes Burma plate.

†Curray *et al.* (1979). Angular velocity doubled to yield full spreading rate; BC denotes Burma plate.

‡Sella *et al.* (2002). IT = ITRF-97.

§Vigny *et al.* (2003). Sign of angular velocity changed for compatibility with Michel *et al.* (2001); IT = ITRF-2000.

(2003), which connected his Euler vector to the other plates using the NUVEL-1a geologic plate motion model (DeMets *et al.*, 1994).

We illustrate the geometry by considering linear velocities (Fig. 11) at 7° N, 92° E, a point on the trench near the center of the rupture. Although only two of the plates are physically present at this point, this construction shows the relationships involved. Relative to Sunda, India moves northeastward at 36 mm/yr. However, Burma moves north-

westward relative to Sunda much faster, and thus northwest relative to India. Hence at this point on the trench, India subducts beneath Burma at about 44 mm/yr in a southeast (106°) direction for the Bird Euler vector, or about 35 mm/yr in the 93° direction for the Curray *et al.* one.

Although this result is not intuitive, it emerges from the relative plate motions unless one or more of them differs significantly from that assumed. This is certainly possible. Our inferred motion of Sunda relative to Eurasia and India

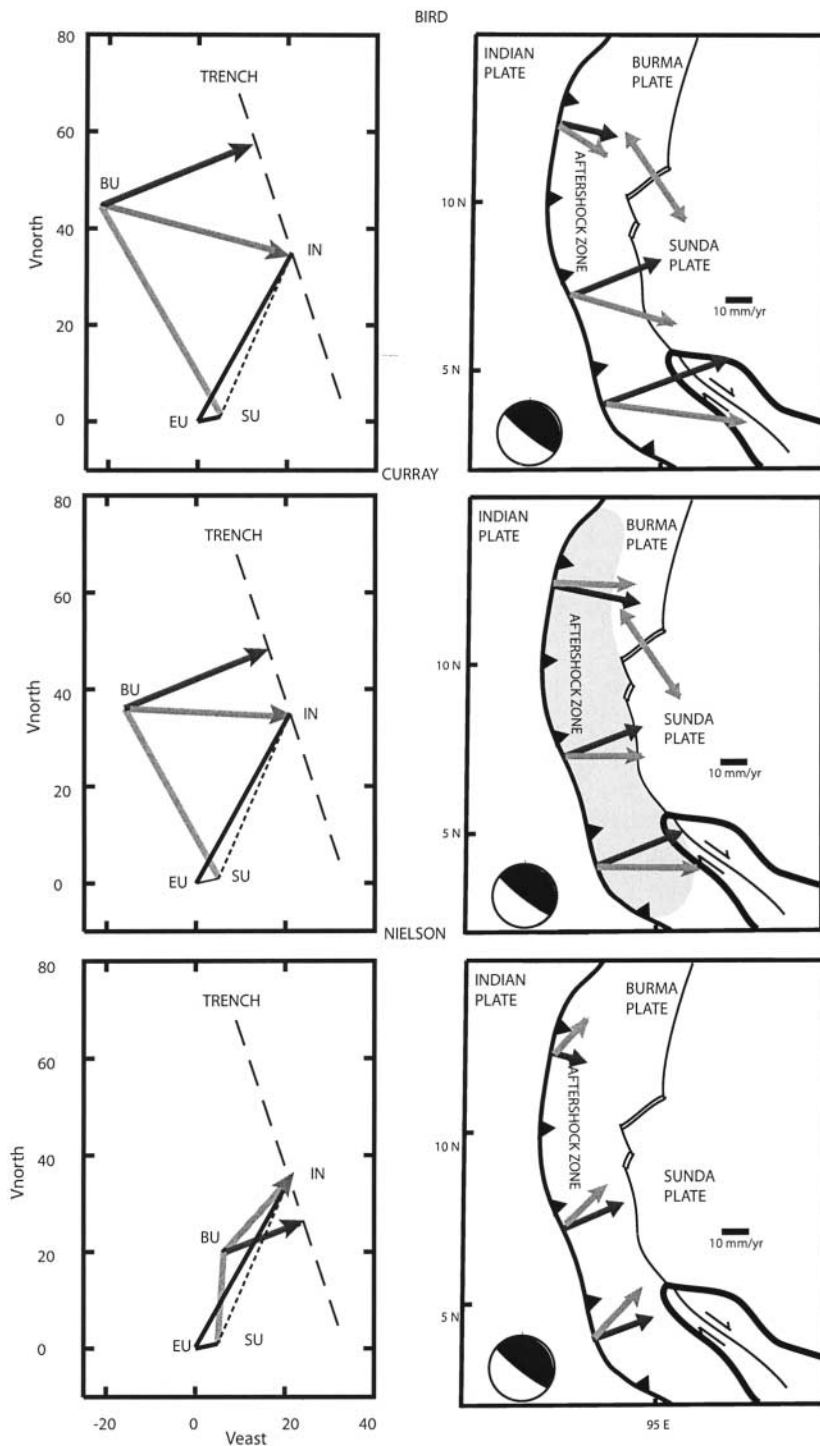


Figure 11. Plate-motion models for the region of the December 2004 earthquake. Top and center rows show results for models in which Burma–Sunda motion is given by Bird (2003) and Curray *et al.* (1979) Euler vectors. Bottom row assumes Burma–Sunda motion is given by Sagaing fault motion. Burma–India motion is shown for total motion and trench-normal component. Left-hand panels show linear velocities at 7° N, 92° E, and right-hand panels show variation along the trench.

differs slightly from that inferred by Chamot-Rooke and Le Pichon (1999) and Michel *et al.* (2001) because for consistency we use the other plates' motion from GPS data, whereas they combine Sunda motion from GPS with the NUVEL-1a geologic plate-motion model (DeMets *et al.*, 1994). The major uncertainty is the Burma–Sunda plate motion, which the Bird and Curray models infer from the rate and direction on the Andaman spreading center. In contrast, Nielson *et al.* (2004) use the 18 mm/yr rate and 355° direction from the Sagaing fault to infer linear velocities further north, at about 16° N. The slower Burma–Sunda motion predicts India moving northeast relative to Burma. Although this would be easier to reconcile with the earthquake mechanism, it implies that either the magnetic data have been misinterpreted or spreading on the Andaman spreading center has slowed and changed direction from that inferred by Curray *et al.* (1979).

As shown in Figure 11 (top and center), the predicted convergence increases southward from 21 mm/yr at 13° N to 55 mm/yr at 4° N for the Bird Euler vector or 28 mm/yr to 39 mm/yr for the Curray vector. The nearly pure thrust fault mechanism (or mechanisms, if the subevents are considered) indicates that the 2004 earthquake reflects primarily the corresponding arc-normal components of convergence, 19–48 or 28–36 mm/yr. Because the poles are nearby, the predicted convergence direction varies along the rupture zone. However, because these poles are not close to the north end of the rupture, we no longer suggest that motion became strike-slip there, explaining why rupture ceased.

The area shows a form of slip partitioning, in which the oblique convergence between India and Sunda gives rise to motion of the Burma microplate. This effect is seen at many trenches where convergence is oblique to the trench and a forearc sliver moves separately from the overriding plate. As a result, earthquake slip vectors at the trench trend between the trench-normal direction and the predicted convergence direction (Jarrard, 1986; Ekström and Engdahl, 1989; DeMets *et al.*, 1990; DeMets and Stein, 1990; McCaffrey, 1991, 1992, 2002) and strike-slip motion occurs between the forearc and the stable interior of the overriding plate. In the limiting case of pure slip partitioning, pure thrust faulting would occur at the trench, and all the oblique motion would be accommodated by trench-parallel strike-slip.

The situation here appears more complicated than typical slip partitioning, however. The slip vector is rotated toward the trench normal (Fig. 11), consistent with partial slip partitioning. Yet, Burma moves northwest faster than expected even for pure slip partitioning (Fig. 12). This peculiarity would favor Nielson *et al.*'s (2004) argument for Burma–Sunda motion slower than inferred from the magnetic anomalies. This possibility is illustrated in Figure 11 (bottom), drawn assuming Burma–Sunda motion is given by the Sagaing fault motion.

A key result of our earlier analysis was that, because the entire aftershock zone slipped, strain accumulated from subduction of India beneath Burma on the northern part of

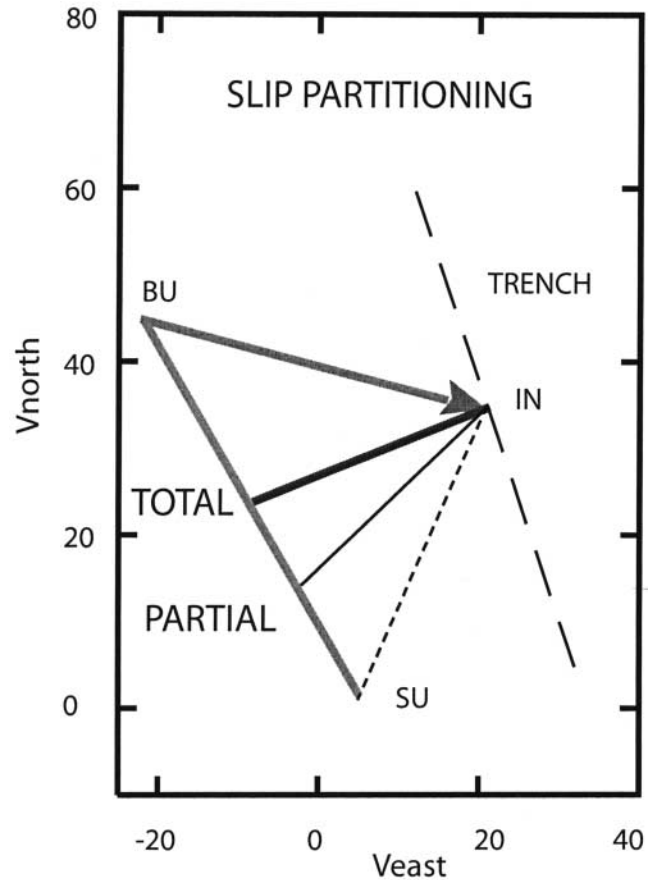


Figure 12. Geometry of slip partitioning assuming India–Sunda motion is taken up by the Burma microplate, showing expected convergence directions and hence earthquake slip vectors for partial and total partitioning. Burma moves northwest, with respect to India, faster than expected, even for pure slip partitioning assuming the magnetic anomalies describe Burma–Sunda motion.

the rupture had also been released. This leaves no immediate danger of a similar oceanwide tsunami being generated by slip on this segment of the plate boundary. If such earthquakes involve at least 10 m of slip, the plate motions predict they should be 200–1000 years apart, with the longer intervals corresponding to failure of the northern portions. Long recurrence times would be consistent with the lack of cultural memory of such events, and initial paleoseismic results from India suggesting a major tsunami about 1000 years ago (Rajendran *et al.*, unpublished manuscript, 2006).

However, we noted the danger of a large tsunami resulting from a great earthquake on segments of the Sumatra trench to the south. McCloskey *et al.* (2005) showed that stress transfer from the December earthquake increased stress on the segment immediately to the south and increased the likelihood of a large earthquake. In fact, an M_w 8.7 earthquake occurred on 28 March 2005, shortly after their article appeared on 17 March. However, it did not generate an oceanwide tsunami because its rupture did not extend to the

seafloor and because of the presence of islands whose uplift does not excite a tsunami (Kerr, 2005b). However, the March event bears out the risk of both local and oceanwide tsunamis generated by the rupture of segments further south (Nalbant *et al.*, 2005), as implied by paleoseismic data (Zachariassen *et al.*, 1999; Natawidjaja *et al.*, 2004).

Implications for Giant Earthquake Occurrence and Tsunami Generation

The December earthquake revived interest in the long-standing question of what are the conditions required for such giant earthquakes and hence oceanwide tsunamis. An important question is whether such earthquakes can occur at any subduction zone, or whether certain combinations of convergence rate, age of the subducting plate, or trench sediment thickness (Ruff and Kanamori, 1980; Ruff, 1989) are required.

We thus re-examined Ruff and Kanamori's (1980) proposal that the largest ($M_w > 8.5$) earthquakes occur only when young lithosphere subducts rapidly. Although this correlation appeared plausible with the data then available ($r = 0.8$), much of the correlation vanishes ($r = 0.4$) (Fig. 13) using new data (Table 2). The largest earthquakes are still on the left (younger) side of the plot, but there is no clear effect of age. The new data contain most of the same earthquakes, but a few are added or updated. For example, the M_w 9.3 of the December 2004 earthquake would not have been predicted. Points for the Chile and Peru trenches shift "downward" because recent plate-motion models derived using either magnetic anomalies (DeMets *et al.*, 1990, 1994) or space geodesy (Norabuena *et al.*, 1998, 1999; Sella *et al.*, 2002) find that Nazca-South America convergence is significantly slower than previously thought. Conversely, GPS rates (Bevis *et al.*, 1995; Calmant *et al.*, 2003) shift the Tonga and Vanuatu points "upward." A further difficulty is that, because large trench events can be normal faults (Kanamori, 1971a), the largest known earthquakes at a trench need not be interplate thrusts. For example, the 1974 M_s 7.5 Lesser Antilles earthquake used in the earlier dataset was a normal fault (Stein *et al.*, 1982). Thus for older events, we face the challenge that not only are their magnitudes poorly known, but they may not have been thrust events. Although paleoseismic evidence can sometimes resolve this issue, many events remain suspect, especially in areas where modern catalogs such as the Harvard CMT dataset contain only very small interplate thrust solutions (e.g., Marianas, Lesser Antilles). Accordingly we use open symbols in Figure 13 for those regions where the largest event is either confirmed or likely to be nonthrust, and reserve solid symbols for those featuring interplate thrust, either documented from a modern seismic solution or strongly suggested by geological evidence, for example, in the 1700 Cascadia earthquake (Satake *et al.*, 2003).

The lack of strong correlation between the maximum size of trench earthquakes and convergence rate and age is

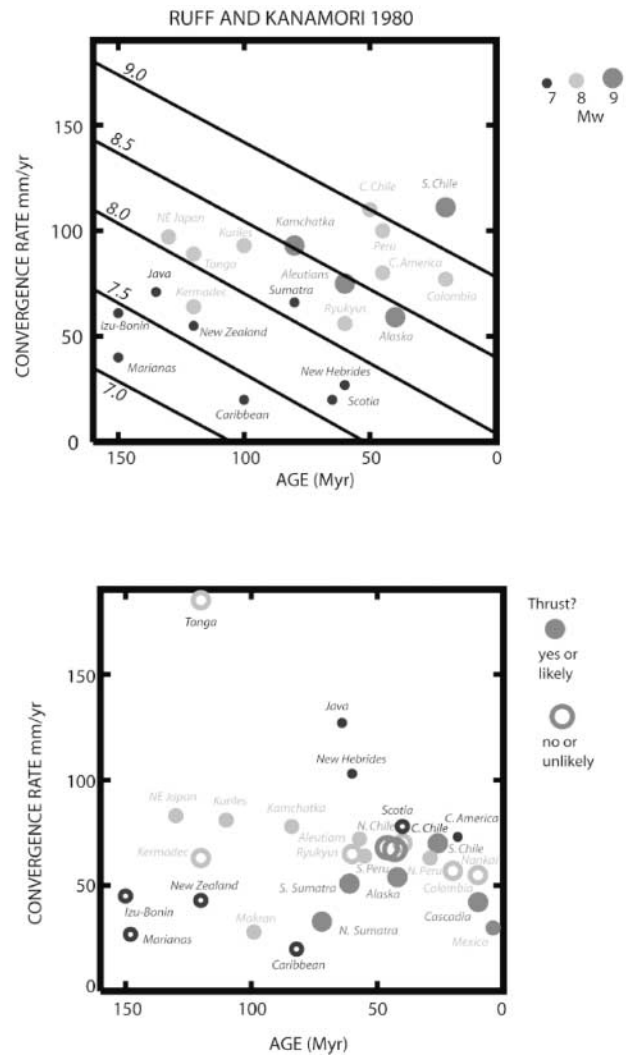


Figure 13. Reanalysis of the proposed dependence of maximum subduction-zone earthquake size on convergence rate and age of the subducting plate. (Top) Dataset used by Ruff and Kanamori (1980) to propose that the largest ($M_w > 8.5$) earthquakes occur only when young lithosphere subducts rapidly. (Bottom) Updated dataset used here, showing much weaker correlation.

consistent with other results. Ruff and Kanamori's (1980) proposal was based on the hypothesis of seismic coupling, in which large earthquakes reflect the mechanical properties of subduction zones. Although the term "seismic coupling" is widely used, a variety of definitions have been offered and its relation (if any) to the mechanics of plate coupling is still unclear (Wang and Dixon, 2004). This hypothesis was originally posed in terms of two end members: coupled Chilean-type zones with large earthquakes and uncoupled Mariana-style zones with largely aseismic subduction (Uyeda and Kanamori, 1979). Hence zones with young, rapidly subducting, and thus warm buoyant lithosphere were expected to be the most strongly coupled in terms of either the largest earthquakes or the highest fraction of the plate motion re-

Table 2
Subduction Zone Convergence Parameters and Maximum Earthquake Magnitudes Used in This Study

Region	Plate Pair [#]	Convergence Rate		Plate Age		Maximum Event			
		mm/yr	Ref.*	Ma	Ref. [†]	Date	M_w	Note [‡]	Ref. [§]
South Chile	NZ-SA	70	R	26	M	1960	9.6	S	a
Central Chile	NZ-SA	70	R	40	M	1922	8.3	M/UM	b
North Chile	NZ-SA	68	R	46	M	1877	9.1	I/UM	c
South Peru	NZ-SA	67	R	43	M	1868	9.2	T/UM	d
North Peru	NZ-SA	63	R	29	M	1940	8.2	S	e
Ecuador-Colombia	NZ-SA	55	R	10	M	1906	8.5	M/UM	b
Central America	CO-CA	73	L	18	M	1992	7.6	S	f
Mexico	RI-NA	30	N	4	M	1932	8.1	M	b
Cascadia	JF-NA	42	N	9	M	1700	9.1	T/G	g
Alaska	PA-NA	54	N	42	M	1964	9.3	S	h
East Aleutian	PA-NA	64	N	55	M	1946	8.6	S	i
West Aleutian	PA-NA	73	N	57	M	1965	8.7	S	j
Kamchatka	PA-NA	78	N	84	Q	1952	8.9	S	k
Kuriles	PA-NA	81	N	110	L	1963	8.5	S	l
Northeast Japan	PA-NA	83	N	130	L	1968	8.2	S	m
Nankai	PH-EU	57	R	20	O	1707	8.8	I/UM	n
Ryukyu	PH-EU	65	R	60	L	1920	8.0	O/UM	o
Izu	PA-PH	45	R	150	L	1947	7.2	O/UM	p
Marianas	PA-PH	27	R	148	L	1929	7.2	O/UM	p
Loyalty-Vanuatu	AU-PA	103	C	60	L	1950	7.8	M/UM	b
Tonga	PA-AU	185	B	120	Q	1865	8.3	T/UM	q
Kermadec	PA-AU	63	R	120	Q	1917	8.1	M/UM	b
New Zealand	PA-AU	43	R	120	Q	1931	7.8	O	p
Java	AU-EU	64	CR	127	M	1994	7.7	S	r
South Sumatra	AU-SU	51	CR	61	M	1833	9.2	G	s
North Sumatra	IN-BU	33	TS	72	M	2004	9.3	S	t
Makran	AR-EU	28	R	99	M	1945	8.1	S	u
Lesser Antilles	NA-CA	20	L	82	M	1974	7.5	O/NF	p,v
South Scotia	SA-SS	78	P	40	M	1924	7.0	O/UM	p

*Rate references: R, REVEL (Sella *et al.* 2002); L, López *et al.* (2006); N, NUVEL-1a (DeMets *et al.*, 1994); C, Calmant *et al.* (2003); B, Bevis *et al.* (1995); CR, Chamot-Rooke and Le Pichon (1999); TS, this study, see text; P, Pelayo and Wiens (1989).

[†]Age references: M, Müller *et al.* (1997); L, Larson *et al.* (1985); O, Ocean Drilling Program, Leg 190; Q, interpolated in magnetic quiet zone from L.

[‡]S, seismological modeling; M, mantle magnitude; I, estimated from macroseismic study; T, tsunami modeling; O, other magnitude (M_s); G, geologic modeling; NF, normal faulting; UM, unknown mechanism.

[§]Seismic moment references: a, Cifuentes and Silver (1989); b, Okal (1992); c, Beck *et al.* (1998); d, Okal *et al.* (2005); e, Beck and Nishenko (1990); f, Dziewonski *et al.* (1993); g, Satake *et al.* (2003); h, Kanamori (1970a); i, López and Okal (2006); j, Wu and Kanamori (1973); k, Kanamori (1976); l, Kanamori (1970b); m, Kanamori (1971b); n, Ando (1974); o, Kanamori (1977b); p, Ruff and Kanamori (1980); q, Okal *et al.* (2004); r, Dziewonski *et al.* (1995); s, Zachariassen *et al.* (1999); t, this study; u, Byrne *et al.* (1992); v, Stein *et al.* (1982).

[#]Plate names: NZ, Nazca; SA, South America; CO, Cocos; CA, Caribbean; RI, Rivera; NA, North America; EU, Eurasia; PA, Pacific; JF, Juan de Fuca; PH, Philippines; AU, Australia; AR, Arabia; IN, India; BU, Burma.

leased as earthquakes. However, although most subduction zones appear to show significant components of aseismic slip, no obvious correlation of the seismic-slip fraction with convergence rate and plate age has been found (Peterson and Seno, 1984; Pacheco *et al.*, 1993).

Although the initially proposed correlations do not seem strong, others remain under investigation. Several studies find a relation between seismic coupling, defined by the seismic-slip fraction, and absolute plate motions, which may affect the mechanics of the interface (Peterson and Seno, 1984; Scholz and Campos, 1995). Another possibility is that thick trench sediments lubricate the interface and allow rupture to propagate long distances, allowing events with $M_w > 8.5$ (Ruff, 1989). Although the initial correlation seems reasonable, there are counterexamples. For example, the Makran

zone has 6000 m of sediment, but the maximum observed M_w is 8, so thick sediment may be a necessary but not sufficient condition. A further complication is that sediment thickness varies along the long rupture zones of such earthquakes.

It is also not clear how sediment affects the trench mechanics. Although strong “seismic coupling,” in general, is assumed to be related to strong mechanical coupling, the converse has also been proposed. Lamb and Davis (2003) argue that such sediment-rich trenches have low stresses on the interface, so these trenches have strong seismic coupling but weak mechanical coupling. They propose that the south Peru and north Chile trench segments, seaward of the high Andes, do not have large trench earthquakes, and so are more strongly coupled mechanically (or less coupled seismically) than segments to the south, such as the south Chile segment

where the 1960 M_w 9.6 earthquake occurred. In their model, Cenozoic climate change deprived the Peru trench of sediment and thus strengthened mechanical coupling there, causing uplift of the high Andes. However, it is not clear that the south Peru and north Chile trench segments differ in seismic coupling from segments to the south. In particular, numerical tsunami modeling shows that the 1868 Peru earthquake ruptured farther to the north than traditionally assumed, implying $M_w \sim 9.2$ (Okal *et al.*, 2006). This observation argues against the location of the high Andes being controlled by unusually strong mechanical coupling.

A significant problem with these arguments is that large trench earthquakes are infrequent, and both the instrumental and historic seismic records are short. As a result, inferring “seismic coupling” from either the size of the largest earthquakes or the seismic-slip fraction is challenging. First, the uncertainties in estimating source parameters of earthquakes from historical data are considerable. Fault areas and amounts of slip must be estimated, and moments and thus magnitudes depend on both these and the rigidity assumed. Second, the seismic cycle is typically much longer than the instrumental record (McCaffrey, 1997), and the size and recurrence interval of earthquakes on a given trench segment can be quite variable (Thatcher, 1990). Third, some large earthquakes have significant slow slip associated with the main event, on timescales of days to years (Kanamori and Cipar, 1974; Cifuentes and Silver, 1989; Barrientos, 1995; Heki *et al.*, 1997). The seismic moment released by these processes, termed slow or silent earthquakes or afterslip, is associated with earthquakes but is not included in conventional seismic-moment calculations, and hence produces a spurious seismic-slip deficit at the plate boundary. Hence, it is difficult to assess whether an apparent seismic-slip deficit indicates a seismic gap where large earthquakes are overdue, or that much of the interplate motion occurs aseismically (Stein, 1992). Fourth, the seismic slip is a fraction of an assumed plate convergence rate, so different plate-motion models give different results (Stein *et al.*, 1986).

We suspect, therefore, that much of the apparent differences between subduction zones, such as some trench segments but not others being prone to $M_w > 8.5$ events, may reflect the short earthquake history sampled. This possibility is supported by the variability in rupture mode at individual trench segments. For example, the Nankai trough history shows that sometimes the entire region slipped in large earthquakes, whereas in other intervals slip divided into smaller events. Although the specific segment sizes that broke are under discussion, various authors agree on the general pattern. Figure 14 shows possible magnitudes for these earthquakes, inferred from a variety of sources (Kanamori, 1972; Ando, 1975; Ishibashi, 1981; Rikitake, 1999). Although none can be assigned with confidence, the relative magnitudes illustrate how the sequence could give rise to earthquakes of quite different magnitudes during different periods. Another example is the trench segment that produced the $M_w \sim 9.6$ 1960 Chilean earthquake. It appears

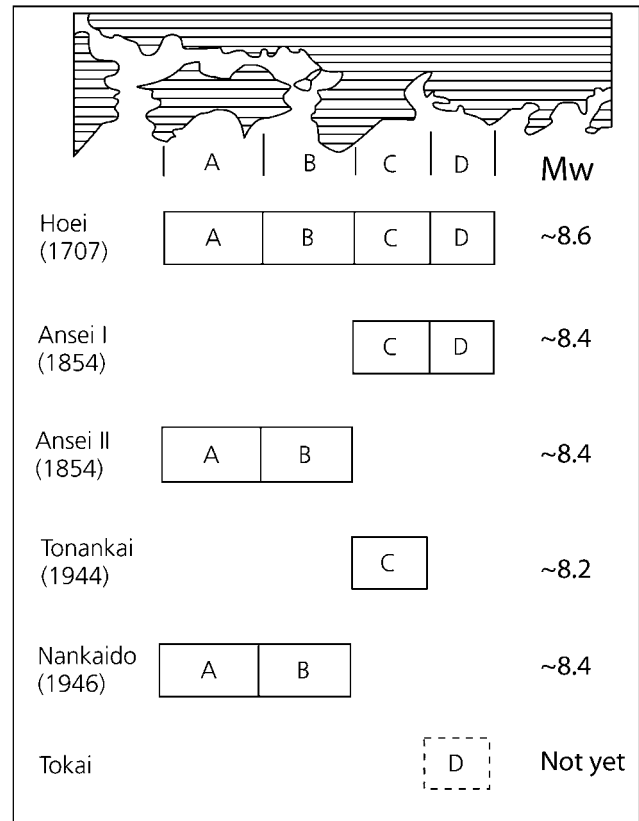


Figure 14. Rupture history for the Nankai trough (Ando, 1975) and possible earthquake magnitudes, illustrating that the sequence could yield earthquakes of quite different magnitudes during different periods.

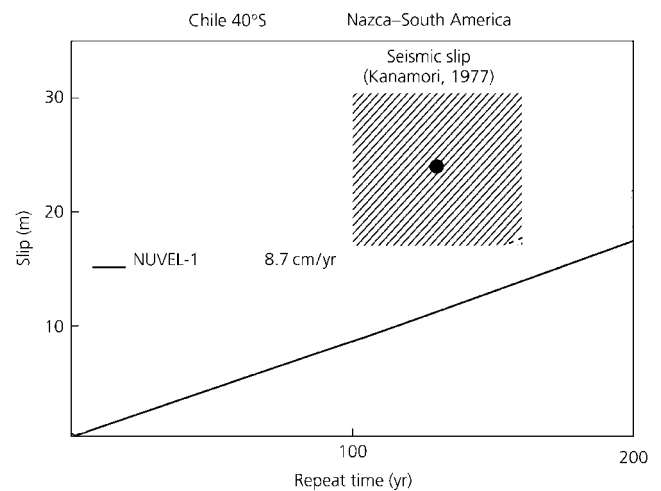


Figure 15. Comparison of the inferred seismic-slip rate (shaded rectangle) and plate-motion rate for the region of the 1960 Chilean earthquake. The fact that the seismic rate exceeds the plate motion implies that it is too high to be a long-term average, suggesting that earlier earthquakes were smaller than the 1960 event, the average recurrence interval is greater than observed in the last 400 years, or both (Stein *et al.*, 1986).

that its rupture mode must be variable because the seismic-slip rate inferred assuming that the 1960 earthquake is this segment's characteristic earthquake exceeds the convergence rate (Fig. 15). Hence Stein *et al.* (1986) proposed that either the characteristic earthquake is smaller than the 1960 event, the average recurrence interval is greater than observed in the past 400 years, or both. Recent paleoseismic studies support this analysis, showing that events in 1737 and 1837 were smaller than the 1960 one, whereas one in 1575 was comparable (Cisternas *et al.*, 2005). Paleoseismic studies also find evidence for variable size of thrust events, presumably due to the differences between multisegment and single-segment rupture, for Cascadia (Kelsey *et al.*, 2005) and the Kuril trench (Nanayama *et al.*, 2003).

Viewed this way, problems resulting from the short earthquake history would not be surprising. If M_w 8 events are three times more common than M_w 8.5, following a Gutenberg–Richter prediction, then $M_w > 8.5$ will be rarer and thus absent from the short record for some trenches. This effect will be enhanced if the larger earthquakes are rarer than this prediction, which is the case globally. As a result, distinguishing real differences among trenches from apparent differences due to the short earthquake history will remain a major challenge. Each new Sumatra-sized earthquake will provide important new data.

Acknowledgments

This research was supported in part by National Science Foundation Grant CMS-03-01054. Several figures were drafted using the GMT package (Wessel and Smith, 1991). We thank Meredith Nettles for access to the Composite Harvard CMT solution before publication.

References

- Aki, K., and P. G. Richards (1980). *Quantitative Seismology: Theory and Methods*, Freeman, W. H. San Francisco, California.
- Ammon, C. J., C. Ji, H.-K. Thio, D. Robinson, S. Ni, V. Hjorleifsdottir, H. Kanamori, T. Lay, S. Das, D. Helmlberger, G. Ichinose, J. Polet, and D. Wald (2005). Rupture process of the 2004 Sumatra-Andaman earthquake, *Science* **308**, 1133–1139.
- Ando, M. (1975). Source mechanisms and tectonic significance of historical earthquakes along the Nankai Trough, Japan, *Tectonophysics* **27**, 119–140.
- Banerjee, P., F. F. Pollitz, and R. Bürgmann (2005). The size and duration of the Sumatra-Andaman earthquake from far-field static offsets, *Science* **308**, 1769–1772.
- Barrientos, S. E. (1995). Dual seismogenic behavior: the 1985 central Chile earthquake, *Geophys. Res. Lett.* **22**, 3541–3544.
- Beck, S. L., and S. P. Nishenko (1990). Variations in the mode of great earthquake rupture along the central Peru subduction zone, *Geophys. Res. Lett.* **17**, 1969–1972.
- Beck, S. L., S. Barrientos, E. Kausel, and M. Reyes (1998). Source characteristics of historic earthquakes along the central Chile subduction zone, *J. South Am. Earth Sci.* **11**, 115–129.
- Ben-Menahem, A., and M. Rosenman (1972). Amplitude patterns of tsunami waves from submarine earthquakes. *J. Geophys. Res.* **77**, 3097–3128.
- Bevis, M., F. W. Taylor, B. E. Schutz, J. Recu, B. Isacks, S. Helu, R. Singh, E. Kendrick, J. Stowell, B. Taylor, and S. Calmant (1995). Geodetic observations of very rapid convergence and backarc extension in the Tonga arc, *Nature* **374**, 249–251.
- Bird, P. (2003). An updated digital model of plate boundaries, *Geochem. Geophys. Geosyst.* **4**, no. 3, doi 10.1029/2001GC000252.
- Byrne, D. E., L. R. Sykes, and D. M. Davis (1992). Great thrust earthquakes and aseismic slip along the plate boundary of the Makran subduction zone, *J. Geophys. Res.* **97**, 449–478.
- Calmant, S., B. Pelletier, P. Lebellegard, M. Bevis, F. W. Taylor, and D. A. Phillips (2003). New insights on the tectonics along the New Hebrides subduction zone based on GPS results, *J. Geophys. Res.* **108**, no. B06, 2319, doi 10.1029/2001JB000644.
- Chamot-Rooke, N., and X. Le Pichon (1999). GPS determined eastward Sundaland motion with respect to Eurasia confirmed by earthquake slip vectors at Sunda and Philippine trenches, *Earth Planet. Sci. Lett.* **173**, 439–455.
- Cifuentes, I. L., and P. G. Silver (1989). Low-frequency source characteristics of the great 1960 Chilean earthquake, *J. Geophys. Res.* **94**, 643–664.
- Cisternas, M., B. F. Atwater, F. Torrejon, Y. Sawai, G. Machuca, M. Lagos, A. Eipert, C. Youlton, I. Salgado, T. Kamataki, M. Shishikura, C. P. Rajendran, J. K. Malik, Y. Riza, and M. Husni (2005). Predecessors of the giant 1960 Chile earthquake, *Nature* **437**, 404–407.
- Curry, J. R., D. G. Moore, L. A. Lawver, F. J. Emmel, R. W. Raitt, M. Henry, and R. Kieckhefer (1979). Tectonics of the Andaman Sea and Burma, in *Geological and Geophysical Investigations of Continental Margins*, Vol. 29, J. S. Watkins, L. Montadert, and P. W. Dickerson (Editors), American Association Petroleum Geologists, Tulsa, Oklahoma, 189–198.
- deGroot-Hedlin, C. D. (2005). Estimation of the rupture length and velocity of the great Sumatra earthquake of Dec 26, 2004 using hydroacoustic signals, *Geophys. Res. Lett.* **32**, no. 11, L11303.
- DeMets, C., and S. Stein (1990). Present-day kinematics of the Rivera plate and implications for tectonics of southwestern Mexico, *J. Geophys. Res.* **95**, 21,931–21,948.
- DeMets, C., R. G. Gordon, D. F. Argus, and S. Stein (1990). Current plate motions, *Geophys. J. Int.* **101**, 425–478.
- DeMets, C., R. G. Gordon, D. F. Argus, and S. Stein (1994). Effect of recent revisions to the geomagnetic reversal time scale on estimates of current plate motion, *Geophys. Res. Lett.* **21**, 2191–2194.
- Dziewonski, A. M., G. Ekström, and M. P. Salganik (1993). Centroid-moment tensor solutions for July–September 1992, *Phys. Earth Planet. Interiors* **79**, 287–297.
- Dziewonski, A. M., G. Ekström, and M. P. Salganik (1995). Centroid-moment tensor solutions for April–June 1994, *Phys. Earth Planet. Interiors* **88**, 69–78.
- Ekström, G., and E. R. Engdahl (1989). Earthquake source parameters and stress distribution in the Adak Island region of the Central Aleutian Islands, Alaska, *J. Geophys. Res.* **94**, 15,499–15,519.
- Geller, R. J. (1976). Scaling relations for earthquake source parameters and magnitudes, *Bull. Seism. Soc. Am.* **66**, 1501–1523.
- Global Centroid Moment Tensor (CMT) Project catalog search, www.globalcmt.org/CMTsearch.html (last accessed January 2006).
- Guilbert, J., J. Vergoz, E. Schissel , A. Roueff, and Y. Cansi (2005). Use of hydroacoustic and seismic arrays to observe rupture propagation and source extent of the $M_w = 9.0$ Sumatra earthquake, *Geophys. Res. Lett.* **32**, no. 15, L15310, doi 10.1029/2005GL022966.
- Guzman-Speziale, M., and J. Ni (1993). The opening of the Andaman Sea: where is the short-term displacement being taken up?, *Geophys. Res. Lett.* **20**, 2949–2952.
- Hanks, T. C., and H. Kanamori (1979). A moment magnitude scale, *J. Geophys. Res.* **84**, 2348–2350.
- Heki, K., S. Miyazaki, and H. Tsuji (1997). Silent fault slip following an interplate thrust earthquake at the Japan Trench, *Nature* **386**, 595–598.
- Holt, W. E., J. Ni, T. C. Wallace, and A. J. Haines (1991). Active tectonics of the eastern Himalayan Syntaxis and surrounding regions, *J. Geophys. Res.* **96**, 14,595–14,632.

- Ishibashi, K. (1981). Specification of a soon-to-occur seismic faulting in the Tokai district, central Japan, based upon seismotectonics, in *Earthquake Prediction, Maurice Ewing Series 4*, D. Simpson and P. Richards (Editors), American Geophysical Union, Washington, D.C., 297–332.
- Ishii, M., P. M. Shearer, H. Houston, and J. E. Vidale (2005). Extent, duration, and speed of the 2004 Sumatra-Andaman earthquake imaged by the Hi-Net array, *Nature* **435**, 933–936.
- Jarrard, R. D. (1986). Terrane motion by strike-slip faulting of forearc slivers, *Geology* **14**, 780–783.
- Ji, C. (2005). Preliminary rupture model of the December 26, 2005 Sumatra earthquake, http://neic.usgs.gov/neis/eq_depot/2004/eq_041226/neic_slav_ff.html (last accessed January 2006).
- Kanamori, H. (1970a). The Alaska earthquake of 1964—radiation of long-period surface waves and source mechanism, *J. Geophys. Res.* **75**, 5029–5040.
- Kanamori, H. (1970b). Synthesis of long-period surface waves and its application to earthquake source studies, Kurile islands earthquake of October 13, 1963, *J. Geophys. Res.* **75**, 5011–5027.
- Kanamori, H. (1971a). Seismological evidence for a lithospheric normal faulting—the Sanriku earthquake of 1933, *Phys. Earth Planet. Interiors* **4**, 289–300.
- Kanamori, H. (1971b). Focal mechanism of the Tokachi-Oki Earthquake of May 16, 1968, *Tectonophysics* **12**, 1–13.
- Kanamori, H. (1972). Tectonic implications of the 1944 Tonankai and the 1946 Nankaido earthquakes, *Phys. Earth Planet. Interiors* **5**, 129–139.
- Kanamori, H. (1976). Re-examination of the Earth's free oscillations excited by the Kamchatka earthquake of November 4, 1952, *Phys. Earth Planet. Interiors* **11**, 216–226.
- Kanamori, H. (1977a). Seismic and aseismic slip along subduction zones and their tectonic implications, in *Island Arcs, Deep-sea Trenches and Back-arc Basins, Maurice Ewing Series 1*, M. Talwani and W. C. Pitman, III (Editors), American Geophysical Union, Washington, D.C., 163–174.
- Kanamori, H. (1977b). The energy release in great earthquakes, *J. Geophys. Res.* **82**, 2981–2987.
- Kanamori, H., and J. J. Cipar (1974). Focal process of the great Chilean earthquake May 22, 1960, *Phys. Earth Planet. Interiors* **9**, 128–136.
- Kelsey, H. M., A. R. Nelson, E. Hemphill-Haley, and R. C. Witter (2005). Tsunami history of an Oregon coastal lake reveals a 4600 year record of great earthquakes on the Cascadia subduction zone, *Geol. Soc. Am. Bull.* **117**, 1009–1032.
- Kerr, R. A. (2005a). Failure to gauge the quake crippled the warning effort, *Science* **307**, 201.
- Kerr, R. A. (2005b). Model shows islands muted tsunami after latest Indonesian quake, *Science* **308**, 341.
- Lamb, S., and P. Davis (2003). Cenozoic climate change as a possible cause for the rise of the Andes, *Nature* **425**, 792–797.
- Larson, R. L., W. C. Pitman, X. Golovchenko, S. C. Cande, J. F. Dewey, W. F. Haxby, and J. L. LaBrecque (1985). *The Bedrock Geology of the World (Map)*, W. H. Freeman, New York.
- Lay, T., H. Kanamori, C. J. Ammon, M. Nettles, S. N. Ward, R. C. Aster, S. L. Beck, S. L. Bilek, M. R. Brudzinski, R. Butler, H. R. DeShon, G. Ekström, K. Satake, and S. Sipkin (2005). The great Sumatra-Andaman earthquake of 26 December 2004, *Science* **308**, 1127–1133.
- López, A. M., and E. A. Okal (2006). A seismological reassessment of the source of the 1946 Aleutian “tsunami” earthquake, *Geophys. J. Int.* **165**, 835–849.
- López, A., S. Stein, T. Dixon, G. Sella, E. Calais, P. Jansma, J. Weber, and P. LaFemina (2006). Is there a Northern Lesser Antilles Forearc block?, *Geophys. Res. Lett.* **33**, no. 7, L07313, doi 10.1029/2005GL025293.
- McCaffrey, R. (1991). Slip vectors and stretching of the Sumatran forearc, *Geology* **19**, 881–884.
- McCaffrey, R. (1992). Oblique plate convergence, slip vectors, and forearc deformation, *J. Geophys. Res.* **97**, 8905–8915.
- McCaffrey, R. (1997). Statistical significance of the seismic coupling coefficient, *Bull. Seism. Soc. Am.* **87**, 1069–1073.
- McCaffrey, R. (2002). Forearc block rotations and plate coupling, in *Plate Boundary Zones*, S. Stein and J. Freymueller (Editors), American Geophysical Union, Washington, D. C., 101–122.
- McCloskey, J., S. S. Nalbant, and S. Steacy (2005). Indonesian earthquake: earthquake risk from co-seismic stress, *Nature* **434**, 291.
- Michel, G., Y. Yu, S. Zhu, C. Reigber, M. Becker, E. Reinhard, W. Simons, B. A. C. Ambrosius, C. Vigny, N. Chamot-Rooke, X. Le Pichon, P. Morgan, and S. Matheussen (2001). Crustal motion and block behavior in SE-Asia from GPS measurements, *Earth Planet. Sci. Lett.* **187**, 239–244.
- Mueller, R. D., W. R. Roest, J.-Y. Royer, L. M. Gahagan, and J. G. Slater (1997). Digital isochrons of the world's ocean floor (http://gdinfo.agg.nrcan.gc.ca/app/agegrid_e.html), *J. Geophys. Res.* **102**, 3211–3214.
- Nalbant, S. S., S. Steacy, K. Sieh, D. Natawidjaja, and J. McCloskey (2005). Earthquake risk on the Sunda trench, *Nature* **435**, 756–757.
- Nanayama, F., K. Satake, R. Furukawa, K. Shimokawa, B. F. Atwater, K. Shigeno, and S. Yamaki (2003). Unusually large earthquakes inferred from tsunami deposits along the Kuril trench, *Nature* **424**, 660–663.
- Natawidjaja, D., K. Sieh, S. N. Ward, H. Cheng, R. L. Edwards, J. Galetzka, and B. W. Suwargadi (2004). Paleogeodetic records of seismic and aseismic subduction from central Sumatran microatolls, Indonesia, *J. Geophys. Res.* **109**, no. B04, B04306, doi 10.1029/2003JB002398.
- Ni, J., M. Guzman-Speziale, M. Bevis, W. E. Holt, T. C. Wallace, and W. R. Seager (1989). Accretionary tectonics of Burma and the three-dimensional geometry of the Burma subduction zone, *Geology* **17**, 68–71.
- Ni, S., H. Kanamori, and D. Helmberger (2005). Energy radiation from the Sumatra earthquake, *Nature* **434**, 582.
- Nielson, C., N. Chamot-Rooke, and C. Rangin and ANDAMAN Cruise Team (2004). From partial to full strain partitioning along the Indo-Burmese hyper-oblique subduction, *Mar. Geol.* **209**, 303–327.
- Norabuena, E., T. Dixon, S. Stein, and C. Harrison (1999). Decelerating Nazca-South America Convergence and Nazca-Pacific spreading, *Geophys. Res. Lett.* **26**, 3405–3408.
- Norabuena, E., L. Leffler-Griffin, A. Mao, T. Dixon, S. Stein, I. S. Sacks, L. Ocala, and M. Ellis (1998). Space geodetic observations of Nazca-South America convergence along the Central Andes, *Science* **279**, 358–362.
- Okal, E. A. (1992). Use of the mantle magnitude M_m for the reassessment of the seismic moment of historical earthquakes. I: Shallow events, *Pure Appl. Geophys.* **139**, 17–57.
- Okal, E. A., and J. Talandier (1989). M_m : a variable-period mantle magnitude, *J. Geophys. Res.* **94**, 4169–4193.
- Okal, E. A., J. C. Borrero, and C. E. Synolakis (2004). The earthquake and tsunami of 17 November 1865: evidence for far-field tsunami hazard from Tonga, *Geophys. J. Int.* **157**, 164–174.
- Okal, E. A., J. C. Borrero, and C. E. Synolakis (2006). Evaluation of tsunami risk from regional earthquakes at Pisco, Peru, *Bull. Seism. Soc. Am.* **96**, 1634–1648.
- Pacheco, J., L. R. Sykes, and C. H. Scholz (1993). Nature of seismic coupling along simple plate boundaries of the subduction type, *J. Geophys. Res.* **98**, 14,133–14,159.
- Park, J., T.-R. A. Song, J. Tromp, E. Okal, S. Stein, G. Roullet, E. Clévéde, G. Laske, H. Kanamori, P. Davis, J. Berger, C. Braitenberg, M. van Camp, X. Lei, H. Sun, H. Xu, and S. Rosat (2005). Earth's free oscillations excited by the 26 December 2004 Sumatra-Andaman earthquake, *Science* **308**, 1139–1144.
- Pelayo, A. M., and D. A. Wiens (1989). Seismotectonics and relative plate motions in the Scotia region, *J. Geophys. Res.* **94**, 7293–7320.
- Peterson, E. T., and T. Seno (1984). Factors affecting seismic moment release rates in subduction zones, *J. Geophys. Res.* **89**, 10,233–10,248.
- Polet, J., and H. Kanamori (2000). Shallow subduction zone earthquakes and their tsunamigenic potential, *Geophys. J. Int.* **142**, 684–702.

- Raju, K., T. Ramprasad, P. Rao, B. Ramalingeswara Rao, and J. Varghese (2004). New insights into the tectonic evolution of the Andaman Basin, northeast Indian Ocean, *Earth Planet. Sci. Lett.* **221**, 145–167.
- Rikitake, T. (1999). Probability of a great earthquake to recur in the Tokai district, Japan: reevaluation based on newly-developed paleoseismology, plate tectonics, tsunami study, micro-seismicity, and geodetic measurements, *Earth Planets Space* **51**, 147–157.
- Royer, J.-Y., and R. Gordon (1997). The motion and boundary between the Capricorn and Australian plates, *Science* **277**, 1268–1274.
- Ruff, L. (1989). Do trench sediments affect great earthquake occurrence in subduction zones?, *Pure Appl. Geophys.* **129**, 263–282.
- Ruff, L., and H. Kanamori (1980). Seismicity and the subduction process, *Phys. Earth Planet. Interiors* **23**, 240–252.
- Satake, K., K. Wang, and B. F. Atwater (2003). Fault slip and seismic moment of the 1700 Cascadia earthquake inferred from Japanese tsunami descriptions, *J. Geophys. Res.* **108**, no. B11, B2535, 17 pp.
- Satyabala, S. P. (2003). Oblique plate convergence in the Indo-Burma (Myanmar) subduction region, *Pure Appl. Geophys.* **160**, 1611–1650.
- Scholz, C. H., and J. Campos (1995). On the mechanism of seismic decoupling and back arc spreading at subduction zones, *J. Geophys. Res.* **100**, 22,103–22,116.
- Sella, G. F., T. H. Dixon, and A. Mao (2002). REVEL: A model for recent plate velocities from space geodesy, *J. Geophys. Res.* **107**, no. B04, doi 10.1029/2000JB000033.
- Stein, S. (1992). Seismic gaps and grizzly bears, *Nature* **356**, 387–388.
- Stein, S., and R. J. Geller (1977). Amplitudes of the split normal modes of a rotating, elliptical Earth excited by a double couple, *J. Phys. Earth* **25**, 117–142.
- Stein, S., and E. A. Okal (2005). Speed and size of the Sumatra earthquake, *Nature* **434**, 581–582.
- Stein, S., J. F. Engeln, C. DeMets, R. G. Gordon, D. Woods, P. Lundgren, D. Argus, C. Stein, and D. A. Wiens (1986). The Nazca-South America convergence rate and the recurrence of the great 1960 Chilean earthquake, *Geophys. Res. Lett.* **13**, 713–716.
- Stein, S., J. F. Engeln, D. A. Wiens, K. Fujita, and R. C. Speed (1982). Subduction seismicity and tectonics in the Lesser Antilles arc, *J. Geophys. Res.* **87**, 8642–8664.
- Thatcher, W. (1990). Order and diversity in the modes of circum-Pacific earthquake recurrence, *J. Geophys. Res.* **95**, 2609–2624.
- Tolstoy, M., and D. B. Bohnenstiehl (2005). Hydroacoustic constraints on the rupture duration, length, and speed of the great Sumatra-Andaman earthquake, *Seism. Res. Lett.* **76**, 419.
- Tsai, V. C., M. Nettles, G. Ekström, and A. M. Dziewonski (2005). Multiple CMT source analysis of the 2004 Sumatra earthquake, *Geophys. Res. Lett.* **32**, no. 17, L17304, doi 10.1029/2005GL023813.
- Tsuboi, S., K. Abe, K. Takano, and Y. Yamanaka (1995). Rapid determination of M_w from broadband P waveforms, *Bull. Seism. Soc. Am.* **85**, 606–613.
- Uyeda, S., and H. Kanamori (1979). Back-arc opening and the mode of subduction, *J. Geophys. Res.* **84**, 1049–1061.
- Vigny, C., W. J. F. Simons, S. Abu, R. Bamphenyu, C. Satirapod, N. Choo-sakul, C. Subarya, A. Socquet, K. Omar, H. Z. Abidin, and B. A. C. Ambrosius (2005). Insight into the 2004 Sumatra-Andaman earthquake from GPS measurements in Southeast Asia, *Nature* **436**, 201–206, doi 10.1038/nature03937.
- Vigny, C., A. Socquet, C. Rangin, S. Abu, N. Chamot-Rooke, M. Pubellier, M.-N. Bouin, G. Bertrand, and M. Becker (2003). Present-day crustal deformation around Sagaing fault, Myanmar, *J. Geophys. Res.* **108**, no. B11, doi 10.1029/2002JB001999.
- Wang, K., and T. H. Dixon (2004). Coupling semantics and science in earthquake research, *EOS Trans. AGU* **85**, 180.
- Weinstein, S. A., and E. A. Okal (2005). The mantle magnitude M_m and the slowness parameter θ : five years of real-time use in the context of tsunami warning, *Bull. Seism. Soc. Am.* **95**, 779–799.
- Wessel, P., and W. H. F. Smith (1991). Free software helps map and display data, *EOS Trans. AGU* **72**, 441, 445–446.
- Wu, F. T., and H. Kanamori (1973). Source mechanism of February 4, 1965, Rat Island earthquake, *J. Geophys. Res.* **78**, 6082–6092.
- Zachariasen, J., K. Sieh, F. W. Taylor, R. L. Edwards, and W. Hantoro (1999). Submergence and uplift associated with the giant 1833 Sumatran subduction earthquake: evidence from coral microatolls, *J. Geophys. Res.* **104**, 895–919.

Department of Geological Sciences
Northwestern University
Evanston, Illinois 60208

Manuscript received 16 January 2006.